A Colorimetric Sensor for the Highly Selective, Ultra-sensitive and Rapid Detection of Volatile Organic Compounds and Hazardous Gases

Li Sun[a], Aurelian Rotaru[b], Koen Robeyns,[a] Yann Garcia *,[a]

[a] Institute of Condensed Matter and Nanosciences, Molecular Chemistry, Materials and Catalysis (IMCN/MOST), Université catholique de Louvain, 1348 Louvain-la-Neuve, Belgium.

[b] Department of Electrical Engineering and Computer Science and MANSiD Research Center, "Stefan cel Mare" University, University Street, 13, Suceava 720229, Romania

Email: yann.garcia@uclouvain.be

Abstract

We present a new colorimetric chemosensor of formula $[Fe(H_2btm)_2(H_2O)_2]Cl_2$ (**1**) (***H_2btm*** = di(1H-tetrazol-5-yl)methane), allowing to detect at real time, with a high selectivity and ultra-sensitivity, 14 different volatile organic compounds (VOCs) and hazardous gases (HGs), in particular amines, which are detected very quickly (< 2 min) with very high sensitivity (0.58 ppm for ammonia (NH_3), 0.62 ppm for hydrazine (NH_2-NH_2), 0.45 ppm for isobutylamine and 0.71 ppm for diethylamine). The detection is accompanied by significant and fast color changes detectable by the naked-eye at ambient conditions. In addition, different VOCs could be distinguished by simple and intuitive standard chemometric means using a handful smartphone-based analytical method, offering a large color panel depending on the detected molecules. The crystal lattice of **1** reconstructs after adsorbing VOCs vapors, reconstruction that is accompanied by a spin state and a color change. In addition to its high thermal stability (up to 170 °C), the colorimetric sensor showed excellent reusability by consecutive 7 cycles of adsorption–desorption. It operates at ambient conditions, is low cost, environmentally friendly, and easy to use, and shows excellent and fast detection performances. Such features offer attractive prospects for **1**, which could be used for *in-field* detection and food safety control in environmental conditions.

1. Introduction

In recent years, more attention has been focused on the efficient detection of chemical pollutants, especially small volatile organic compounds (VOCs) and hazardous gases (HGs).[1,2] This is very challenging because VOCs are relatively volatile at room temperature, even at low concentration levels. Generally speaking，it enters the body through normal breathing, and can cause serious teratogenic, mutagenic and carcinogenic effects, which can damage human organs.[3] In addition, sources of VOCs are various since one can find them in building materials, dry cleaning fluid, paints, lacquers, varnishes, copying and printing machines, or produced by burning of fuels, to name but a few.[4] As we know, alcohols, one of the highest volatile organic solvents, have been reported to be absorbed by the living body through inhalation, ingestion and dermal exposure.[5] When inhaled, alcohol-vapor molecules completely bypasses our digestive system, which would cause irritation and even lung damage, which can lead to long-term breathing problems and a higher risk of lung infections.[6] Needless to say, amines, one of the most common VOCs, are highly toxic even at low concentrations. Amines are an irritant to eyes, skin and the respiratory tract. Inhalation of vapor-phase amines can oxidize hemoglobin which becomes methemoglobin, causing it to lose its oxygen-carrying function, thereby damaging both the central nervous and cardiovascular systems.[7] Children may be even more susceptible to the respiratory effects of amines than adults. On the other hand, accidental leaking of different toxic and hazardous industrial chemicals from factories seriously threatens the human health, although these incidents rarely happen. For instance, $NH_{3(g)}$ and its derivatives are toxic and hazardous, volatile, irritating and corrosive compounds, which can lead to bronchiolar and alveolar edema, and airway destruction resulting in respiratory distress or failure.[8] Wherefore, from the viewpoint of building a healthy and friendly living environment for human beings, the detection of VOCs and HGs is thus very significant.

Currently, related conventional detection technologies mainly include chromatography (such as gas chromatography, high-performance liquid chromatography, and ion chromatography), spectroscopy (spectrophotometry), biological detection, etc.[9-11] However, the above-mentioned technologies, generally, involve expensive equipment and a complicated analysis process, and are unsuitable for *in-field* or real-time testing. Therefore, it would be remarkable to develop a novel sensor technology that would be low cost, environmentally friendly, and easy to operate, and that would offer excellent and fast detection performances.

Chemosensors based on sensor technology for the selective and sensitive detection of VOCs and HGs by oversimplified patterns, are one of the research hotspots in analytical chemistry.[12,13] More importantly, a chemosensor must be able to detect VOCs and HGs, and produce an easily measurable response, such as a color change, an electronic signal, a magnetic signal or any other macroscopic property.[14] Thus, due to their low cost, high sensor response and simple operation, optical chemosensors based on functional materials have been much tracked in the past few decades.

Among sensors, porous coordination polymers (PCPs) (or metal-organic frameworks (MOFs)) have been suggested because they tend to exhibit high porosity and offer the opportunity to explore the interaction between the framework and molecules within the same platform.[15,16] Another substance class concerns metal oxide semiconductors (MOS) which have be shown to be popular for detecting HGs and VOCs. For instance, Liu *et al*[17] prepared SnO_2-based sensors exhibiting high selectivity and sensitivity, fast response rate, reliable reversibility, and relevant stability toward ethanol at low concentrations, but operating at high temperatures (in the region of 100-250°C). On other grounds, some Fe(II) complexes, have been shown to switch their spin states/color, depending on gas vapours or direct solvent contact.[18-23] These so-called Fe(II) spin crossover complexes,[24] show limited color sets corresponding to their high-spin (HS) and low-spin (LS) states, and hardly maintain their color in ambient conditions due to the release of guest species at atmospheric pressure.

Detection and discrimination among a wide range of toxic and hazardous guest vapor molecules by a detectable color change remains a current challenge and the topic of substantial amounts of recent research. Recently, Garcia *et al.* reported on a mononuclear Fe(II) neutral complex chemically responsive pigment with the ability to differentiate four different TICs and methanol/ethanol among other alcohols.[25,26] This system is now modified to a unique colorimetric chemosensor with the formula $[Fe(H_2btm)_2(H_2O)_2]Cl_2$ (**1**) (***H_2btm*** = di(1H-tetrazol-5-yl)methane), allowing to detect at real time, with a high selectivity and ultra-sensitivity, VOCs and HGs under ambient conditions, by the naked-eye, which is ground breaking. In particular, it rapidly detects and discriminates vapors of $NH_{3(g)}$ and amines, in the gas-phase, by showing different colors. The study of the mechanism revealed a conformation spin state switching after adsorption. Furthermore, a friendly smartphone-based analytical method was developed to make **1** accessible for *in-field* applications. Most interestingly, an obvious color change was observed upon guest contact and recorded, by outputting RGB_1 (red, green, blue) and HSB_2 (hue, saturation, brightness) values directly. The recorded data were then

analyzed by a simple and intuitive standard chemometric means (HCA = hierarchical clustering analysis). Forasmuch, it indicates that **1** has broad application prospects in environmental protection and food safety assessment, as an *in-field* naked-eye colorimetric sensor.

2. Experimental Section

2.1. Material and Measurements

All chemicals and solvents were purchased from commercial sources of analytical grade and used without further purification. All chemical reagents (hydrochloric acid (37%), ethyl acetate, methanol (MeOH), ammonia ($NH_3 \cdot H_2O$), hydrazine monohydrate ($N_2H_4 \cdot H_2O$), isobutylamine, 3-picolylamine, furfurylamine, triethylamine, 1,2-diaminocyclohexane, diethylenetriamine, hexylamine, diethylamine, ethylenediamine, 1,2-diaminopropane and pyridine) were purchased from VWR and Avantor. Malononitrile was purchased from Fluorochem. Iron(II) chloride tetrahydrate ($FeCl_2 \cdot 4H_2O$), zinc chloride anhydrous ($ZnCl_2$), sodium azide (NaN_3), and magnesium sulfate anhydrous ($MgSO_4$) were purchased from Acros Organics. Ascorbic acid was purchased from Alfa Aesar. The characterization methods and the instruments are shown in S1. The synthesis of ***H_2btm*** is shown in S2.

2.2 Synthesis of $[Fe(H_2btm)_2(H_2O)_2]Cl_2$ (1)

Di(1H-tetrazol-5-yl)methane (***H_2btm***, 76.0 mg, 0.50 mmol) was dissolved in diluted hydrochloric acid solution (15%, 2 mL) at room temperature. $FeCl_2 \cdot 4H_2O$ (50.0 mg, 0.25 mmol) with a pinch of ascorbic acid was dissolved in a hydrochloric acid solution (15%, 1 mL), and then added to the ligand solution, creating a light-yellow solution. This solution was mechanically stirred for 3 min at 60 °C and left to crystallize at ambient conditions. Small pale-blue block crystals were collected by filtration after 1 day and dried in air. Yield: 82 mg (0.18 mmol, 70%). Elemental analysis for $C_6H_{12}FeN_{16}O_2Cl_2$ (467.07 g/mol) (%): Calcd. C, 15.43; H, 2.59; N, 47.96; Found: C, 15.94; H, 2.78; N, 48.13.

2.3 Detection of VOCs

For testing vapochromism, a home-made set-up was used (see Scheme S1). About 20 mg of **1** in a little dish was added to a cell culture dish containing 0.3 mL (by another little dish) of different VOCs solvents. These were covered by a lid and incubated for 1 min to 120 min at ambient conditions. The discoloration pictures were recorded at different times and concentrations. Then, the pictures were converted into digital information *via* the application (Color Name AR, V. Polyanskiy, Color Name App, iOS 11.0, 2020) of iPhone X. The

application is capable to output RGB_1 (red, green, blue) and HSB_2 (hue, saturation and brightness) values directly. These data were analyzed by standard chemometric means, using a hierarchical clustering analysis (HCA). This method detects VOCs not only *in situ* but also in real time by the naked-eye. After adsorbing vapor molecules of NH_3, N_2H_4, isobutylamine, etc., **1** was named **1**@NH_3, **1**@N_2H_4, **1**@isobutylamine, and so on. In order to increase the surface area for diffusion and therefore shorten the experiment time, crystals of **1** were systematically ground.

3. Results and Discussion

3.1. Structure Description of 1

Pale-blue block single crystals of **1** were obtained from the reaction of ***H_2btm*** and $FeCl_2{\cdot}4H_2O$ in 15% HCl aqueous solution at room temperature after 1 day. Single-crystal X-ray diffraction analysis reveals that **1** crystallizes in the form of a pale-blue block in the monoclinic space group *$P2_1/c$*, located on an inversion center, with two formula units per unit cell and a calculated density of 1.864 g cm^{-3} at 297 K. From Figure 1a, the Fe(II) center is octahedrally coordinated by two aqua ligands in axial positions and by two neutral ***H_2btm*** molecules in the plane (Fe1−N12 = 2.2044 (13) Å, Fe1−N2 = 2.1522 (13) Å). The bond length from the metallic centre and the coordinated water molecules is slightly shorter 2.0870(12) Å. The coordination octahedron is slightly distorted (O13 − Fe1−N12 = 91.82(5)°, ∠ O13−Fe1−N2 = 93.79(5)°, and ∠N12−Fe1−N2 = 83.62(5)°). The packing of **1** as viewed along the *a*-axis is shown in Figure1b: expansion of the hydrogen bonds generates a 2D sheet along the bc plane. Both OH hydrogens interact with chlorine anions, which further interact with a tetrazole N-H. The other tetrazole NH hydrogen bonds with a neighboring tetrazole ring (Figure 1c). Space filling representation of the packing of **1** demonstrates the absence of channels within the lattice (Figure1d). The structure of **1** is isostructural to the Co and Ni reported analogues.[27] Details on the measurement and refinement data are given in Table S1.

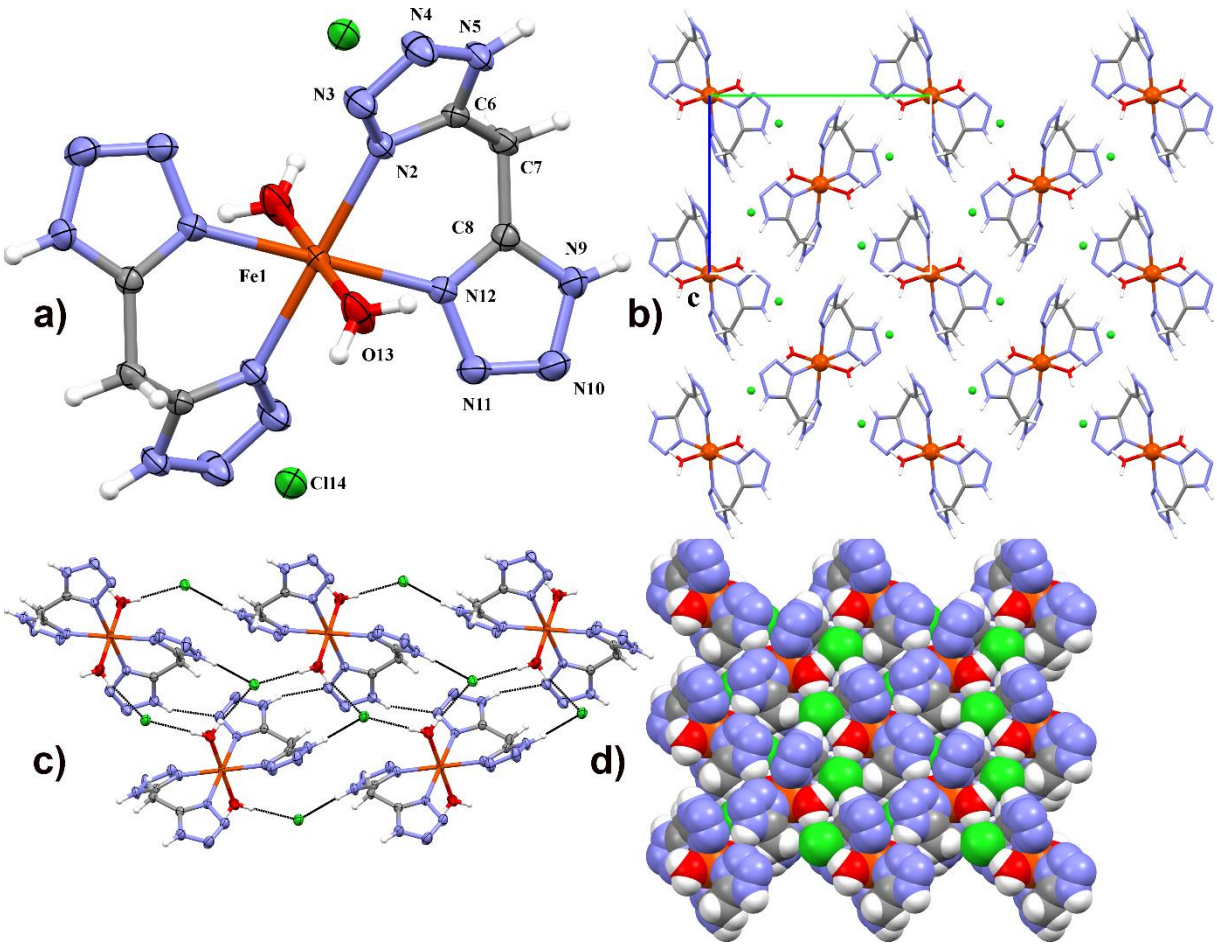

Figure 1. (a) Molecular unit of $[Fe(H_2btm)_2(H_2O)_2]Cl_2$ (**1**). (b) Stick representation of **1** as viewed along the *a*-axis of the crystal packing, showing the counter ions of Cl^- (green ball). (c) Hydrogen bonding diagram of **1** within the 2D hydrogen bonded layer along the bc plane. (d) Space-filling model of **1** as viewed down the *a*-axis.

3.2 Characterization of 1 before and after Vapors Contact

1 was subjected to a variety of VOCs gas-phase molecules including common solvents, acids and even molecular compounds containing amines functional groups. Different colors were distinguished including violet (ethylenediamine, 1,2-diaminopropane), green (e.g. 2-chloroaniline), brown (nitric acid), orange (pyridine), pink (formaldehyde), red (ammonia and hydrazine) at room temperature, by the naked-eye (Figure 2). Most interestingly, the sensibility of the detection has been investigated and the response time has been considerably improved.

Figure 2. Images depicting vapochromic transformation on the sensing of VOCs by complex **1** for 120 min. at room temperature, on ground crystals.

3.2.1 Stability Analysis of 1

Thermogravimetric (TGA) and Differential Thermal Analysis (DTA) curves of **1** are shown in Figure 3. The heating rate was 5 °C min^{-1} in a nitrogen atmosphere in open Al_2O_3 crucibles, containing 14.83 mg of **1**. In the DTA plot, a melting point peak emerged at 202 ºC, followed by an endothermic process which can be seen over the range 156-216 ˚C (Figure 3b). From the TGA plot (Figure 3a), a continuous mass loss occurs as the temperature is increased from room temperature and is particularly rapid in the 156-216 ˚C range, the percentage of total mass loss being ~15%. At 202 ˚C, the mass loss corresponds to two water molecules. A second intense exothermic decomposition stage was seen in the DTA curve between 216 to 248 ºC and a peak was observed at 239 ˚C. The TGA curve showed a mass loss of 15.6%. A third and fourth

weaker exothermic peak can be seen at 262 ^{o}C and 358 ^{o}C, respectively. The percentage of total mass loss were ~14% and 10%, respectively. However, in a smoother fashion than before. The thermal stability was found to be high, more than 170 °C. Furthermore, since the guest phase molecules adsorb on the surface of **1**, as concluded from the FT-IR analysis of **1** toward different vapors (Figure S1), this indicates, to a certain extent, that VOCs vapor molecules do affect the vibrational structure and the position of the spectrum of **1**. However, there is no significant change to the skeleton structure and functional groups of **1** during the adsorption of different guest gas-phase molecules.

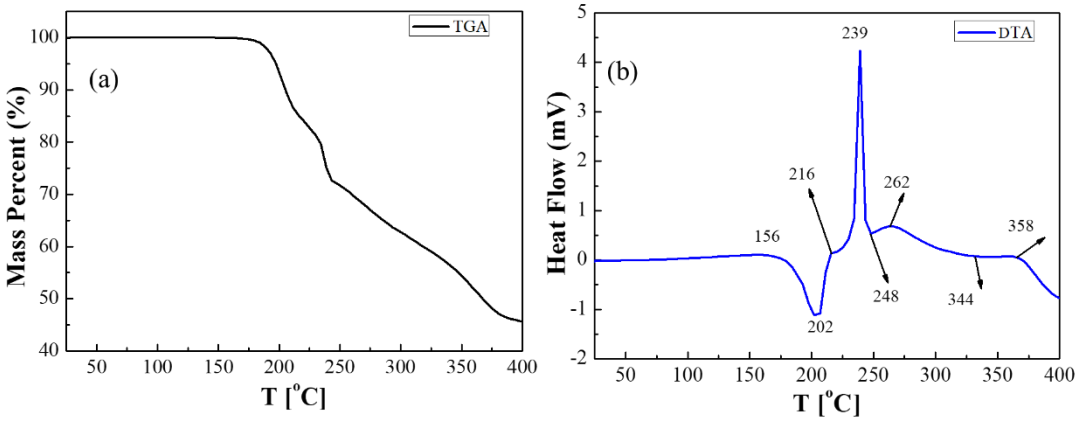

Figure 3 (a) TGA and (b) DTA plots of **1** over the range of 25-400 °C.

3.2.2 Ultraviolet−Visible Diffuse Reflectance Spectroscopy (DRS) Analysis of 1 Towards Different Vapors

We have shown that **1** is an efficient gas-induced color chemosensor operating at room temperature and in the solid state. Different colors were distinguished by the naked-eye after guest contact (see Figure 2). The visible change in color is attributed to the shift of the charge transfer transition during the spin state switch to a lower energy after adsorbing VOCs gas-phase molecules.[28] As observed in Figure 4, the diffuse reflectance spectrum of **1** after adsorbing VOCs obtained at room temperature exhibits an intense band at around λ = 270 nm, in addition to new broad bands at λ = 530 nm. Based on the literature for Fe(II) complexes in similar ligand environments,[29,30] the absorption band λ = 270 nm was assigned to ligand-centered n−π* transition. The broad bands at λ = 530 nm, being more intense for LS Fe(II) compounds,[31] can be assigned to the $^{1}A_{1}\rightarrow{}^{1}T_{1}$ d−d transition of the LS state of Fe(II).[26] For

1@NH_3 and **1**@1,2-diaminopropane the spectra at around λ = 530 nm are the most obvious. Similar adsorption points after adsorbing a series of analogue molecules are shown in Figure S3. This indicates that the introduction of an electron-donating ammonia group leads to a change in the π-withdrawing ability of the azole-type ligand, thus influencing the spin state population of **1**.

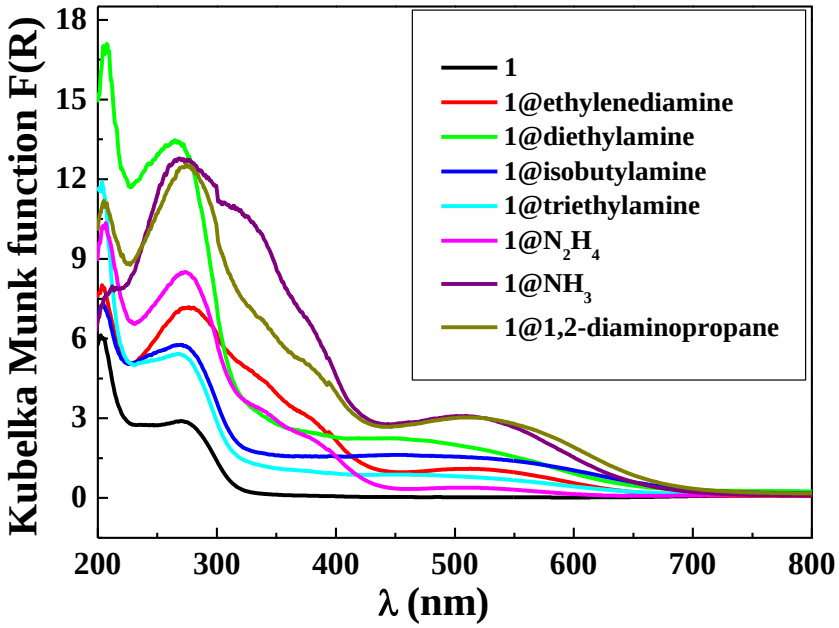

Figure 4 Diffuse-reflectance spectroscopy of **1** before and after adsorption of different guest molecules at room temperature.

3.2.3 ^{57}Fe Mössbauer Spectroscopy Analysis of 1 Towards Different Vapours

^{57}Fe Mössbauer spectra of **1** have been recorded before and after guests inclusion at room temperature (Figure 5 and Figure S4). A quantitative analysis of spin-state and oxidation state could be undertaken (Table S2). ^{57}Fe Mössbauer spectra of **1**, at 298 K, show one quadrupole doublet with an isomer shift δ = 1.15(1) mm s^{-1} and a quadrupole splitting ΔE_Q = 3.66(1) mm s^{-1} of area fraction A = 100%, where the parameters are typical for HS Fe(II) ions (Figure 5a).[32,33] After adsorbing $NH_{3(g)}$ molecules, **1**@NH_3 (Figure 5b), a new quadrupole doublet emerges in the centre [δ = 0.38(1) mm s^{-1}; ΔE_Q = 0.23(1) mm s^{-1}] of area fraction A = 70%. These parameters are characteristic of LS Fe(II) ions in a FeN_6 core. Indeed, replacement of the oxygen atoms by nitrogen atoms, which are less electronegative, increase the electronic density of s electrons in the vicinity of the iron nucleus and thereby decreases the isomer shift.[34] The

remaining contribution corresponds to the HS Fe(II) site: HS [δ = 1.08(1) mm s^{-1}; ΔE_Q = 3.51(3) mm s^{-1}; and area fraction A = 30%]. Not all Fe sites are switched, which could be due to crystallographic modifications that restrict further $NH_{3(g)}$ molecules diffusion. For **1**@N_2H_4 (Figure 5f) and **1**@isobutylamine (Figure 5e), it shows new quadrupole doublet with δ = 0.39(3) mm s^{-1} and δ = 0.38(1) mm s^{-1}, with ΔE_Q = 0.20(5) and 0.08(3) mm s^{-1}, respectively. These parameters are typical for LS Fe (II) ions, indicating that **1** absorbs $N_2H_{4(g)}$ and isobutylamine$_{(g)}$ molecules to form a part of LS FeN_6 centre. In addition, quadrupole doublets centered at δ = 1.00(1) and 1.08(3) mm s^{-1} with ΔE_Q = 2.57(1) and 3.59(1) mm s^{-1}, respectively, are observed. These parameters are assigned to HS Fe(II) ions without any sign of oxidation. ΔE_Q values of **1**@triethylamine (Figure 5g) and **1**@diethylamine (Figure 5h) are 0 mm s^{-1}, which indicates that the structure of the material is completely symmetrical after adsorbing triethylamine$_{(g)}$, diethylamine$_{(g)}$. Mössbauer spectra of **1**@1,2-diaminopropane (Figure 5d), **1**@ethylenediamine (Figure 5c), **1**@hexylamine (Figure S4d), show quadrupole doublets with δ = 0.40(1), δ = 0.39(1) and δ = 0.36(4) mm s^{-1}, as well as ΔE_Q = 0.22(2), ΔE_Q = 0.20(3) and ΔE_Q = 0.26(1) mm s^{-1}, (area fraction A = 53%, 41% and 9%, respectively), which are unambiguously due to LS Fe(II) ions of **1** after adsorption. The original HS Fe(II) doublets have area fractions of 47%, 59% and 91%, respectively, as well as isomer shifts δ = 1.09(1), 1.08(1) and 1.09(1) mm s^{-1} and a slightly smaller ΔE_Q = 3.60(1), 3.59(1) and 3.59(1) mm s^{-1} (arising from a decreased population of low lying d-orbitals decreasing the valence electron contribution to the electric field gradient). Interestingly, **1** can also selectively senses a series of analogue molecules (Figure S4). This indicates that the invasion of gas-phase VOCs molecules causes redistribution of 3*d* orbital electrons of Fe(II), leading to a part of HS states to be converted to the LS states. Furthermore, the radius of nitrogen atoms is smaller than that of oxygen atoms, and the electronegativity is also smaller. So, it is easy to form a strong coordination field between N and Fe(II) ions. There is no doubt that N atoms of VOCs molecules replace O atoms and coordinate with the central iron atom (on the surface of the crystals) after **1** is exposed to VOCs gas-phase molecules, thereby, constructing a LS FeN_6 core together with the azole ligands from HS FeN_4O_2. Such results are consistent with the one originating from DRS. Details of Mössbauer parameters are given in Table S2.

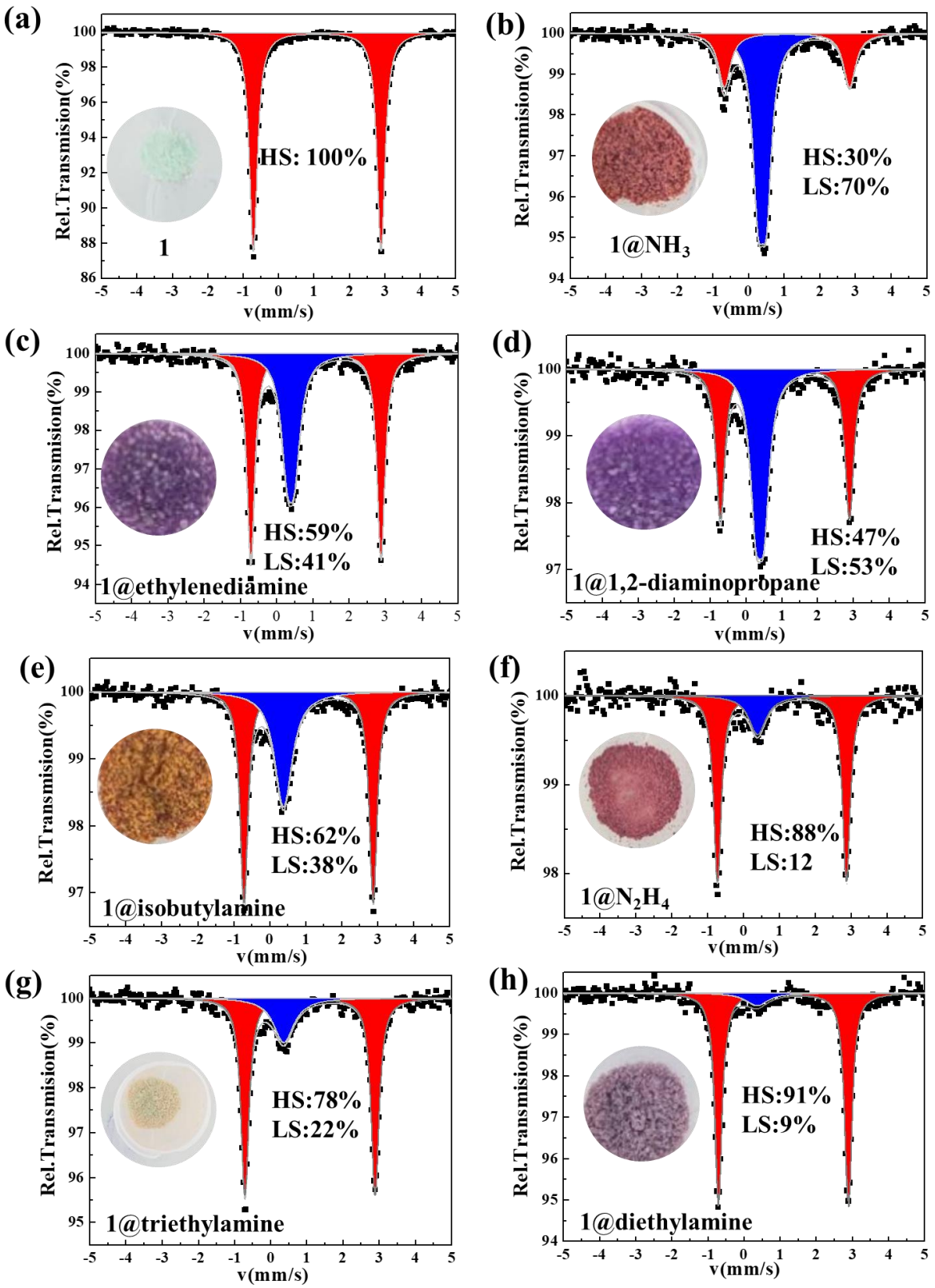

Figure 5 Spin-state population at room temperature by ^{57}Fe Mössbauer spectroscopy of (a) **1** (b) **1**@NH_3 (c) **1**@ethylenediamine (d) **1**@1,2-diaminopropane (e) **1**@isobutylamine (f) **1**@N_2H_4 (g) **1**@triethylamine (h), and **1**@diethylamine.

3.2.4 Magnetic Properties Analysis of 1 Towards Different Vapours

The changes in spin state observed for the various transformations described above provide this material with potential as a spin-based chemosensor. This is further investigated by variable-temperature magnetic susceptibility measurements on polycrystalline samples after VOCs gas-phase adsorption over the range of 4−400 K under a constant field of 1 T. From Figure 6 and Figure S5, SQUID magnetometry demonstrates lower χT values for samples after VOCs adsorption compared to **1** at 298 K, which show a full paramagnetic state with χT = 3.60 cm^3 K mol^{-1}, corresponding to Fe(II) ions (S = 2, HS state), which is consistent with the observations from single crystal X-ray diffraction. For instance, **1**@NH_3, showed a dramatic modification of its spin state since it is mostly diamagnetic at 300 K with χT = 0.50 cm^3 K mol^{-1}, in agreement with Mössbauer data. Upon heating from 298 to 400 K, χT was found to increase, presumably due to solvent release which involves a change in spin state, although not all. The observations directly prove that a spin state switching process accompanies the adsorption or desorption of ammonia and VOCs guest-phase molecules of **1**. Foremost, magnetic properties of **1** after adsorption of other VOCs are consistent with ^{57}Fe Mössbauer spectroscopy data.

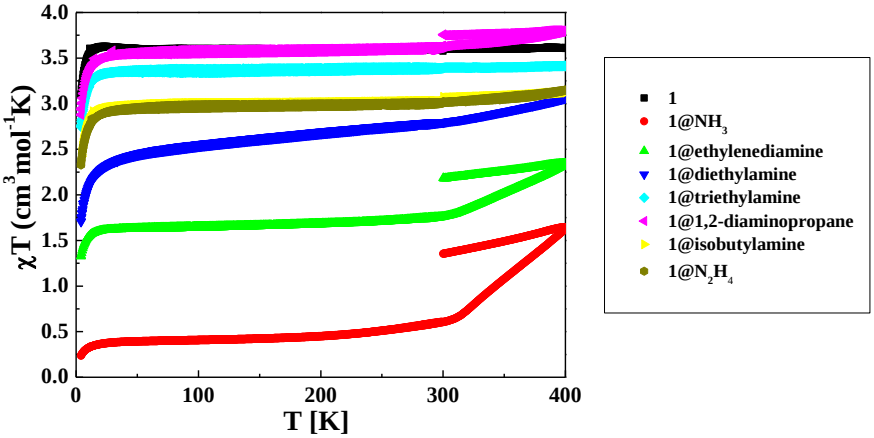

Figure 6 Temperature-dependent χT plots for **1** before (black) and after adsorption of different guest molecules.

3.3 Detection of VOCs

3.3.1 Selectivity of the VOCs Colorimetric Sensor

As observed by the naked-eye, **1** can detect and distinguish a wide range of hazardous VOCs at room temperature (Figure 2). In order to undertake a simple and effective comparison by recording the color change of **1** for each guest analyte, we have used an application to convert

sensor pictures printed on smartphones into a digital information. Therefore, there was no need to keep the discolored images. We have used the most simple and effective statistical method to record and analyze collected data, called hierarchical cluster analysis (HCA) which is a classification scheme based on the Euclidean distance (the Euclidean distance between two points in Euclidean space is the length of a line segment between the two points) of data points in their full dimensions.[35] It uses, in addition, minimum variance for clustering (which is known as the 'Ward's method').[36] Each experiment is defined as a six-dimensional vectors， which are composed of six RGB_1 (red, green and blue) and HSB_2 values (hue, saturation and brightness). These data are used to quantitatively compare the color changes of images from Figure 2.[25,37,38] Then, we are simply comparing the spatial distance by HCA between the observed colors "before" and "after" VOCs contact, the color-change profiles being inherently digital data which can therefore be easily handled by routine chemometric analysis. HCA is based on the Euclidean distance between these vectors in this six-dimensional RGB_1 and HSB_2 value space, thereby, generating a dendrogram, as shown in Figure 7. A cut-off at a distance level of 200 gives a distribution of materials in five homogeneous classes with common characteristics clearly marked and interpretable (Figure 7). There are five groups of 33 samples, which imply five kinds of colors after adsorption.[39] The raw digital color vectors from a total of 18 experimental trials are given in Table S3.

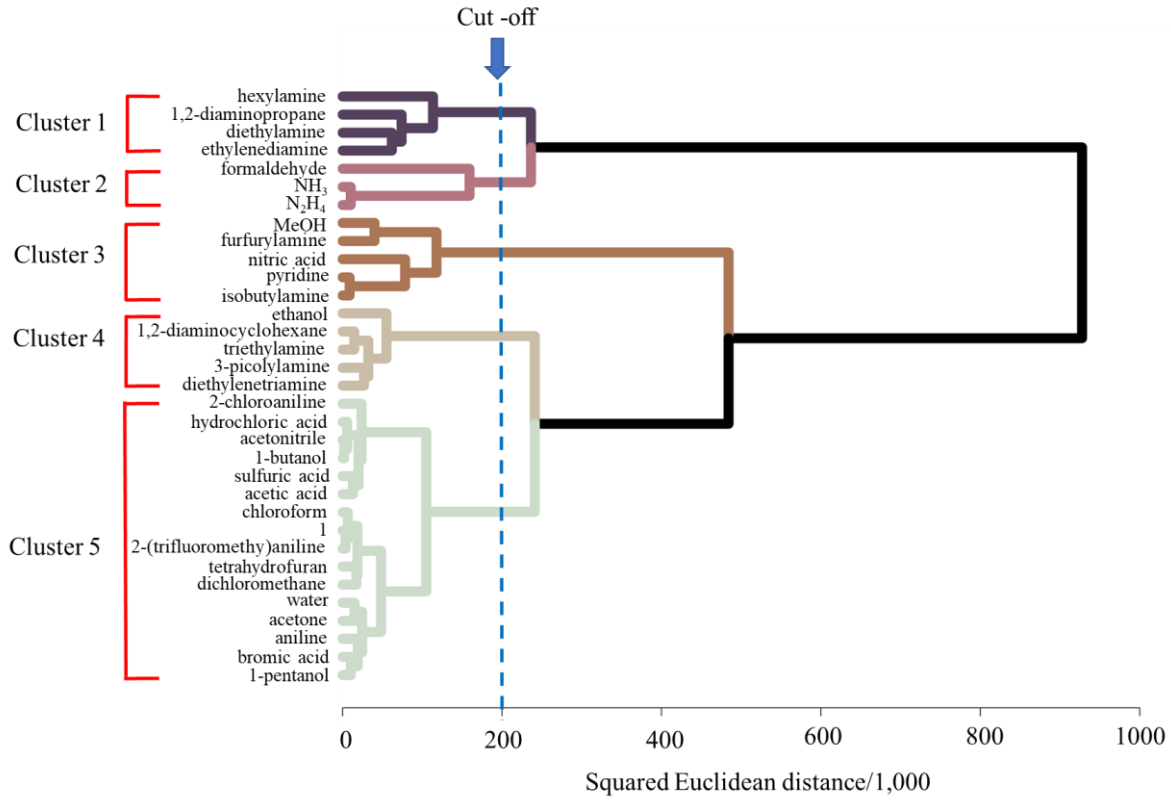

Figure 7 HCA for 32 VOCs at saturation concentrations and a control. All experiments were performed in triplicate: no confusion could be observed in the classification for 18 trials. The Euclidean distance corresponds to the total length of the six-dimensional color vector shown in Table S3.

It takes a few seconds to identify some hazardous VOCs from the sensor color change, and 90% of the response can be observed in less than 10 min., as shown in Figure 8 for 14 representative VOCs. Among them, the fastest color change was observed for diethylamine, isobutylamine, hydrazine, ammoniac and triethylamine (Figure S6a). The sensor detects $NH_{3(g)}$ molecules at room temperature, which turns to pink in seconds, and then red within minutes. For $N_2H_{4(g)}$, it also turns light-pink in seconds, but it is more slowly changing to pink compared to $NH_{3(g)}$. Amazingly, when complex **1** was exposed to isobutylamine$_{(g)}$ at room temperature, it instantly turns from colorless to pale-pink, and then begins to turn pale-red within 10 min, and finally, transform into orange-yellow when the material was saturated with isobutylamine$_{(g)}$ to give **1**@isobutylamine (Figure 9a). The situation differs with diethylamine$_{(g)}$, which turns to pink in seconds after adsorption, and then changed to purple after few minutes. Other tested VOCs show longer response time (Figure S6b and Figure S6c). These observations indicate that under identical conditions, the vapor pressure of different VOCs influence the absorption speed of the sensor, and therefore the resulting color.[25] The result also shows that the smaller the molecular structure ($NH_{3(g)}$), the faster the changing colors. It is likely that small molecules are easily coordinated with the exposed central metal atoms on the surface. In addition to the above-mentioned, different ligands have different coordination capabilities due to differences in steric hindrance and electron donating capabilities, which in turn leads to different speeds of sensor color change. Generally speaking, the coordination capabilities of nitrogen-containing ligands are stronger than other ligands. At the same time, diffusion kinetics of the gas-phase ligand will also cause the difference in the adsorption kinetics of the sensor. Therefore, the speed of color change is the result of a variety of factors. In contrast, without statistical analysis, the VOCs (N_2H_4, NH_3, isobutylamine and diethylamine) could be determined from these unique colors even by the naked-eye, such as red, pink, orange-yellow and purple, respectively in Figure 2. In all, it indicates that **1** could be used as a potential chemosensor, without any expensive equipment and complicated analysis system, for *in-field* detection of $NH_{3(g)}$ molecules.

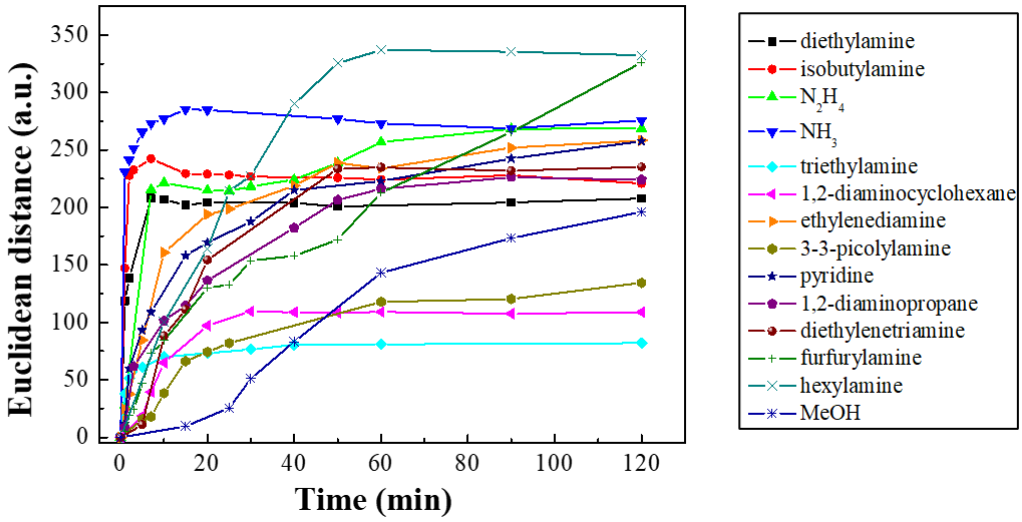

Figure 8 Response time of the sensor. Total Euclidean distance *vs* time for 14 representative VOCs at statured concentrations; All experiments were performed in triplicate: no confusion could be observed in the classification for 18 trials. The Euclidean distance corresponds to the total length of the 6-dimensional color vector shown in Table S4.

3.3.2 Sensitivity of the VOCs Colorimetric Sensor by Naked Eyes

In order to evaluate the sensitivity of the VOCs colorimetric sensor (**1**), distinct concentrations of guest gas-phase molecules (isobutylamine, N_2H_4, NH_3 and diethylamine) were tested at room temperature. After exposure to various concentrations of VOCs vapours (0-50 ppm) for 10 min, the color change of **1** was recorded by our smartphone application. The colorimetric sensor gradually turned its color, which was easily observed by the naked-eye. It can be concluded from Figure 9a that the color of **1** changed from colorless to dark-red, then to orange-yellow with the increase of isobutylamine$_{(g)}$ concentration from 0 to 50 ppm. Interestingly, as the concentration of $N_2H_{4(g)}$ increases, the color of **1** changed from pale-blue to pink in Figure S7a1. Pink-red color appeared due to the increase in the concentration of $NH_{3(g)}$ from 0 to 50 ppm in Figure 9b. The color of **1** changed from pale-blue to pink, and finally dark-red in Figure S7a2 after adsorption of concentrations of diethylamine in the range of 0 to 50 ppm. It is very convenient to distinguish the color of the **1** with diethylamine$_{(g)}$ concentration of 0.71 ppm from that of the blank one in Figure S7a2. However, when the diethylamine concentration is 0.44 ppm, the color of the sensor is very similar to that of the blank one. Thereby, the limit of detection (LOD) of the chemosensor to diethylamine$_{(g)}$ was found to be 0.71 ppm (0.62 ppm for N_2H_4, 0.45 ppm for isobutylamine and 0.58 ppm for $NH_{3(g)}$, respectively) by the naked-eye (Figure 9 and Figure S7). Therefore, the proposed Fe(II)-based colorimetric sensor could be used for quantitative assay of several molecules, some varying in

detection color. In particular, it is worthwhile to note that according to the literature,[8] a concentration of NH_3 vapours of 14 ppm can cause upper respiratory tract injuries, and exposure to a concentration of 55 ppm for 1 min is very dangerous, and can even cause death. Thus, **1** could rapidly detect NH_3 at concentration levels below the health risk limit.

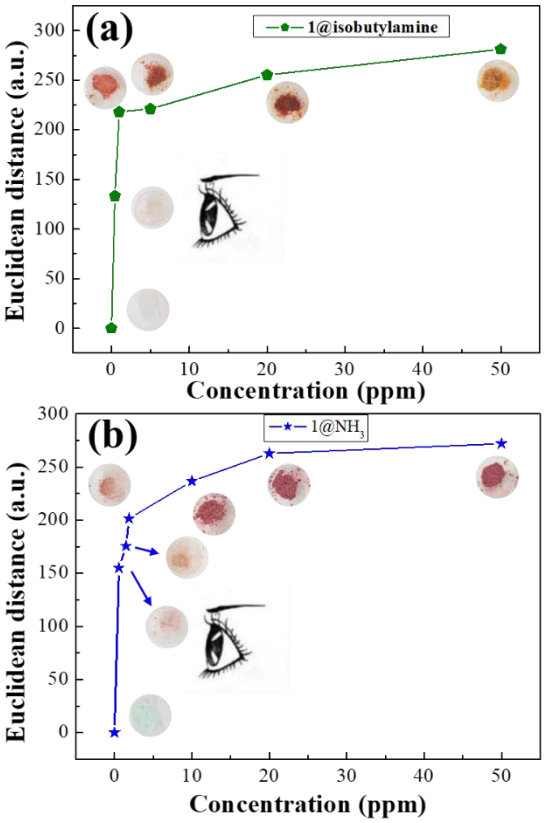

Figure 9 Images depicting vapochromic transformation on the sensing of (a) isobutylamine (b) NH_3 by complex **1** at different concentration, and effect of the initial concentration of isobutylamine and NH_3 on color changing of **1** for 10 min. at room temperature. The ratio of Euclidean distance versus VOCs concentration in the range of 0 to 50.0 ppm. The Euclidean distance corresponds to the total length of the 6-dimensional color vector shown in Table S5.

3.3.3 Regeneration of Colorimetric Sensor

A more detailed regeneration process of colorimetric sensor (**1**) is provided in Supporting Information section S3. As displayed in Figure 10 and Figure S8c, after 7 cycles of adsorption-desorption, the Euclidean distance of the sensor for $NH_{3(g)}$ changed slightly at room temperature and the Euclidean distance values remain similar after 7 cycles. The regeneration ability was also demonstrated with 1,2-diaminopropane$_{(g)}$ and methanol$_{(g)}$ as shown in Figure S8a and S8b, respectively. After 4 cycles of adsorption-desorption, the Euclidean distance was not modified. Moreover, the high stability of sensor **1** toward the acid was demonstrated with $HCl_{(g)}$ (Figure

S9b.) As can be seen, no modification is observed by comparison of the Mössbauer spectrum before (Figure S9a) and after HCl exposure (Figure S9b). Both spectra show a 100% HS Fe(II) population without any sign of oxidation (e.g. the absence of Fe(III) species). A similar spectrum was obtained on Figure S9c with 100% Fe(II) species, after having adsorbed $NH_{3(g)}$ on our sensor which was washed with 4%HCl solution. Thus, our coordination compound has high stability over bases (e.g. NH_3). Thence, our coordination compound not only has high stability over a wide pH range, but also display excellent regeneration performance (Figure 10 and Figure S8).

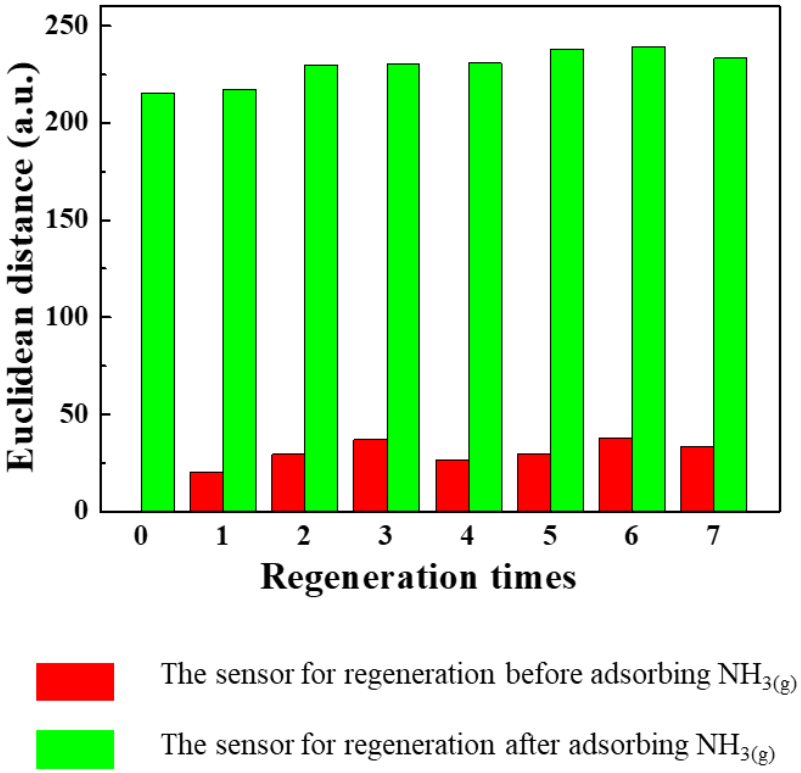

Figure 10 Diagram of reusability test for the colorimetric sensor on the regenerated at room temperature. All experiments were performed in triplicate: no confusion could be observed in the classification for 18 trials. The Euclidean distance corresponds to the total length of the 6-dimensional color vector shown in Table S6.

3.3.4 Smartphone-Based Colorimetric Read-Out

A regression analysis was performed using an empirical formula to correlate VOCs-concentrations and Euclidean distance, which is calculated from RGB_1 (red, green, blue) and HSB_2 (hue, saturation and brightness) values collected *via* a smartphone, as shown in Figure S9. It shows a good fit between experimental data and the model with the non-linearity of R^2 = 0.97 for isobutylamine$_{(g)}$ concentration ranging from 0 to 50 ppm (R^2 = 0.91 for $N_2H_{4(g)}$, R^2 = 0.94 for diethylamine$_{(g)}$ and R^2 = 0.94 for $NH_{3(g)}$). From 0 - 5 ppm in Figure S9a, the Euclidean

distance increases as the concentration increases, and reaches a plateau when the concentration is more than 5 ppm. Most of the VOCs have a danger level when the concentration is more than 5 ppm. Therefore, the sensor can be a good thing to do the warning. In addition, the linearity between 0 and 5 ppm can be used for predicting the gas concentration under the safe range. which can be used for risk assessment. We digitalized the read-outs of colorimetric sensor **1** with a smartphone which has a color analysis application. When we use **1** to detect gas-phase VOCs, the application can record the color change of **1** and export RGB_1 (red, green, blue) and HSB_2 (hue, saturation and brightness) values of the color. Finally, the RGB_1 (red, green, blue) and HSB_2 (hue, saturation and brightness) values are analyzed by the computational algorithm (HCA) to obtain fitting parameters and the calibration plot. This discovery demonstrates a potential application of combining a colorimetric sensor and digitalized analyzer— which could be a cheaper and more portable way than the traditional chromatography and can be used for *in-situ* analysis of gas-phase VOCs.

3.4 Discoloration Mechanisms of Sensor 1 to Detect VOCs with Amine Groups

The crystals of **1** turned to tarnish after absorbing VOCs molecules, even after recrystallization, thus preventing any single crystal X-ray diffraction determination. However, according to the analysis and characterization results, in particular from Mössbauer and UV-vis diffuse reflectance spectroscopies and SQUID magnetometry, we found that Fe(II) of **1** switched from the HS to LS state after absorbing VOCs molecules. The main reason is that the guest molecules cause change in the field strength around the central Fe(II) ions and modify the charge density. Combining other analysis results, we speculate that there might be two interactions that cause color changes in **1** (Figure 11): (i) The guest molecules coordinate with the exposed central atom Fe(II) ions on the surface of **1**, after replacing its water molecules. The electronegativity as well as the radius of the N atom being smaller than that of the O atom, makes it easy to coordinate a ligand (with N atom), which set a strong ligand field. [25,26] (ii) The ***H₂btm*** ligand is a rich-nitrogen heterocyclic ring. When the guest-molecular structure is very large, due to the steric hindrance effect, the water molecule cannot be replaced. However, the ligand can form hydrogen bonds with the guest molecule with amino groups (supported by Table S7). Under the influence of these interactions, the color of **1** change after adsorbing VOCs gas-phase molecules.

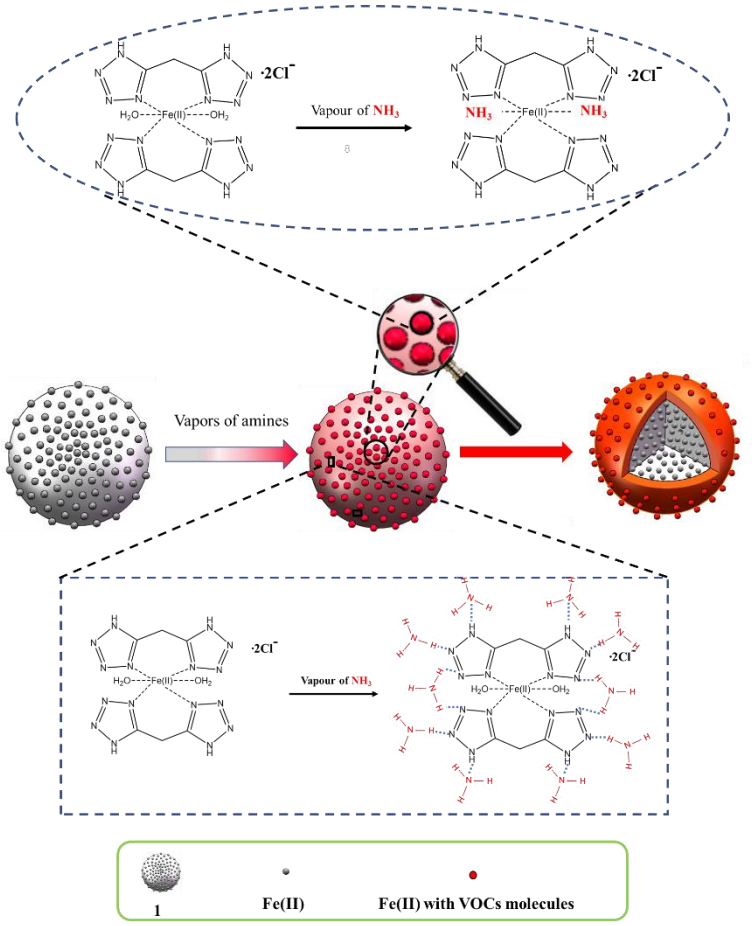

Figure 11. Suggested discoloration mechanism of amines for **1**.

4. Conclusions

In summary, a colorimetric pigment **1** containing high density of uncoordinated N atoms for the fast, highly selective and sensitive detection of a wide range of analytes has been reported for the first time. Interestingly, the colors of **1** change particularly fast (< 2 min) after adsorbing VOCs molecules with —NH_2 groups. Moreover, it can be distinguished by the naked-eye without the need for cryogenic equipment or temperature pre-treatment at room temperature. In addition, the central Fe(II) atoms of **1** form different electron distribution states after adsorbing VOCs, especially $NH_{3(g)}$ and amines, which switch from HS to LS electronic states, leading to colors change. Classification analysis reveals that the HCA has an extremely high dimensionality and, consequently, the ability to discriminate among a large number of VOCs over a wide range of concentrations. A good relationship (R^2 = 0.97) between Euclidean distance and isobutylamine concentrations from 0.45 ppm to 50 ppm indicated that the sensor can be used for quantitative assay of VOCs. Furthermore, we integrated our Fe(II)-based colorimetric sensor detection with a smartphone. The developed strategy is portable and accessible for *in field* analysis and does not requires advanced instruments. This colorimetric

sensor **1** is still in the initial stage and is only used for the detection of certain specific substances. However, due to its rapid, highly selective, sensitive and quantitative detection function, it has shown broad prospects for future applications. This opens up prospects for the development of this compound as potential sensor for small molecules in the gas-phase, by combining a portable mobile phone system and the HCA analysis method.

ASSOCIATED CONTENT

Supporting Information

The Supporting Information is available free of charge on the ACS Publications website. Overview of FT-IR, Powder X-ray diffractograms, Diffuse-reflectance spectroscopy, ^{57}Fe Mössbauer spectroscopy parameters, Temperature-dependent χT plots and Euclidean distance of **1** before and after adsorption of different guest molecules at room temperature.

Acknowledgements

This work was supported through the Fonds De La Recherche Scientifique—FNRS (CDR 33694457, PDR T.0095.21), the Ministère de l'Education et de la Recherche de Roumanie and WBI. L. S. was supported by fellowship from the China Scholarship Council (201804910584). We are highly thankful to Dr. M. Chen for her input on the Hierarchical Cluster Analysis and Cuilian Liu for useful discussions.

References

1. Mirzaei, A.; Leonardi, S. G.; Neri, G. Detection of hazardous volatile organic compounds (VOCs) by metal oxide nanostructures-based gas sensors: A review. *Ceram. Int.* **2016**, *42*, 15119-15141.

2. Chen, W. Y.; Jiang, X.; Lai, S. N.; Peroulis, D.; Stanciu, L. Nanohybrids of a MXene and transition metal dichalcogenide for selective detection of volatile organic compounds. *Nat. Commun.* **2020**, *11*, 1302-1311.

3. Kampa, M.; Castanas, E. Human health effects of air pollution. *Environ. Pollut.* **2008**, *151*, 362-367.

4. Feng, Z.; Ma, Y.; Natarajan, V.; Zhao, Q.; Ma, X.; Zhan, J. In-situ generation of highly dispersed Au nanoparticles on porous ZnO nanoplates via ion exchange from hydrozincite for VOCs gas sensing. *Sensor. Actuat. B-Chem.* **2018**, *255*, 884-890.

5. Rydosz, A.; Maciak, E.; Wincza, K.; Gruszczynski, S. Microwave-based sensors with phthalocyanine films for acetone, ethanol and methanol detection. *Sensor. Actuat B-Chem.* **2016**, *237*, 876-886.

6. Anjum, S. R.; Narwade, V. N.; Bogle, K. A.; Khairnar, R. S. Graphite doped Hydroxyapatite nanoceramic: Selective alcohol sensor. *Nano-Structures and Nano-Objects* **2018**, *14*, 98-105.

7. Noh, H. L.; Park, Y. K.; Oh, B. M.; Zheng, J.; Kim, S.-H.; Lee, W.; Kim, J. H. Colorimetric chemosensor for detection of a volatile organic compound, ethylamine, under versatile conditions: Solution, thin-film, and dyed fabric. *Sensor. Actuat. B-Chem.* **2019**, *301*, 127079.

8. Liu, X.; Chen, N.; Han, B.; Xiao, X.; Chen, G.; Djerdjc, I.; Wang, Y. Nanoparticle cluster gas sensor: Pt activated SnO_2 nanoparticles for NH3 detection with ultrahigh sensitivity. *Nanoscale* **2015**, *7*, 14872-14880.

9. Lan, H.; Rönkkö, T.; Parshintsev, J.; Hartonen, K.; Gan, N.; Sakeye, M.; Sarfraz, J.; Riekkola, M.-L. Modified zeolitic imidazolate framework-8 as solid-phase microextraction Arrow coating for sampling of amines in wastewater and food samples followed by gas chromatography-mass spectrometry. *J. Chromatogr. A* **2017**, *1486*, 76-85.

10. Kamarei, F.; Ebrahimzadeh, H.; Asgharinezhad, A. A. Optimization of simultaneous derivatization and extraction of aliphatic amines in water samples with dispersive liquid-liquid microextraction followed by HPLC. *J. Sep. Sci.* **2011**, *34*, 2719-2725.

11. Elbashir, A. A.; Ahmed, A. A.; Ahmed, S. M. A.; Aboul-Enein, H. Y. 1,2-Naphthoquinone-4-Sulphonic Acid Sodium Salt (NQS) as an Analytical Reagent for the Determination of Pharmaceutical Amine by Spectrophotometry. *Appl. Spectrosc. Rev.* **2012**, *47*, 219-232.

12. Wang, S. L.; Li, C.; Song, Q. H. Fluorescent Chemosensor for Dual-Channel Discrimination between Phosgene and Triphosgene. *Anal. Chem.* **2019**, *91*, 5690-5697.

13. Qian, J.; Wen, C.; Xia, J. Development of highly efficient chemosensors for Cu^{2+} and N_2H_4 detection based on 2D polyaniline derivatives by template-free chemical polymerization method. *J. Hazard. Mater.* **2020**, *389*, 121902.

14. Wenger, O. S. Vapochromism in organometallic and coordination complexes: chemical sensors for volatile organic compounds. *Chem. Rev.* **2013**, *113*, 3686-3733.

15. Zhang, M.; Feng, G.; Song, Z.; Zhou, Y. P.; Chao, H. Y.; Yuan, D.; Tan, T. T.; Guo, Z.; Hu, Z.; Tang, B. Z.; Liu, B.; Zhao, D. Two-dimensional metal-organic framework with wide channels and responsive turn-on fluorescence for the chemical sensing of volatile organic compounds. *J. Am. Chem. Soc.* **2014**, *136*, 7241-7244.

16. Yu, Y.; Ma, J. P.; Zhao, C. W.; Yang, J.; Zhang, X. M.; Liu, Q. K.; Dong, Y. B. Copper(I) Metal-Organic Framework: Visual Sensor for Detecting Small Polar Aliphatic Volatile Organic Compounds. *Inorg. Chem.* **2015**, *54*, 11590-11592.

17. Xiao, L.; Xu, S.; Yu, G.; Liu, S. Efficient hierarchical mixed Pd/SnO_2 porous architecture deposited microheater for low power ethanol gas sensor. *Sensor. Actuators B-Chem.* **2018**, *255*, 2002-2010.

18. Bartual-Murgui, C.; Akou, A.; Thibault, C.; Molnár, G.; Vieu, C.; Salmon, L.; Bousseksou, A. Spin-crossover metal–organic frameworks: promising materials for designing gas sensors. *J. Mater. Chem. C* **2015**, *3*, 1277-1285.

19. Rodriguez-Jimenez, S.; Feltham, H. L.; Brooker, S., Non-Porous Iron(II)-Based Sensor: Crystallographic Insights into a Cycle of Colorful Guest-Induced Topotactic Transformations. *Angew. Chem. Int. Edit.* **2016**, *55*, 15067-15071.

20. Vinogradova, K. A.; Pishchur, D. P.; Korolkov, I. V.; Bushuev, M. B. Magnetic properties and vapochromism of a composite on the base of an iron(II) spin crossover complex. *Inorg. Chem. Commun.* **2019**, *105*, 82-85.

21. Urien, E. R.; Burzurı, E.; Bartolome, E. F.; Tunon, M. A. G. G.; Presa, P. d. l.; Poloni, R.; Teat, S. J.; Cost, J. S. A switchable iron-based coordination polymer toward reversible acetonitrile electro-optical readout. *Chem. Sci.* **2019**, *10*, 6612-6616.

22. Garcia, Y.; van Koninbsruggen, P. J.; Lapouyade, R.; Fournès, L.; Rabardel, L.; Kahn, O.; Ksenofontov, V.; Levchenko, G.; Gütlich, P. Influences of Temperature, Pressure, and Lattice Solvents on the Spin Transition Regime of the Polymeric Compound $[Fe(hyetrz)_3]A_2 \cdot 3H_2O$ (hyetrz = 4-(2'-hydroxyethyl)-1,2,4-triazole and A^- =3-nitrophenylsulfonate). *Chem. Mater.* **1998**, *10*, 2426-2433.

23. Costa, J. S.; Jiménez, S. R.; Craig, G. A.; Barth, B.; Beavers, C. M.; Teat, S. J.; Aromí, G. Three-way crystal-to-crystal reversible transformation and controlled spin switching by a nonporous molecular material. *J. Am. Chem. Soc.* **2014**, *136*, 3869-3874.

24. Gütlich, P.; Garcia, Y.; Goodwin, H. A., Spin crossover phenomena in Fe(ii) complexes. *Chem. Soc. Rev.* **2000**, *29*, 419-427.

25. Guo, Y.; Xue, S.; Dîrtu, M. M.; Garcia, Y. A versatile iron(ii)-based colorimetric sensor for the vapor-phase detection of alcohols and toxic gases. *J. Mater. Chem. C* **2018**, *6*, 3895-3900.

26. Naik, A. D.; Robeyns, K.; Meunier, C. F.; Léonard, A. F.; Rotaru, A.; Tinant, B.; Filinchuk, Y.; Su, B. L.; Garcia., Y. Selective and reusable iron(II)-based molecular sensor for the vapor-phase detection of alcohols. *Inorg. Chem.* **2014**, *53*, 1263-1265.

27. Freis, M.; Klapötke, T. M.; Stierstorfer, J. r.; Szimhardt, N. Di(1H-tetrazol-5-yl)methane as Neutral Ligand in Energetic Transition Metal Complexes. *Inorg. Chem.* **2017**, *56*, 7936-7947.

28. Xue, S.; Guo, Y.; Rotaru, A.; Muller-Bunz, H.; Morgan, G. G.; Trzop, E.; Collet, E.; Olah, J.; Garcia, Y. Spin Crossover Behavior in a Homologous Series of Iron(II) Complexes Based on Functionalized Bipyridyl Ligands. *Inorg. Chem.* **2018**, *57*, 9880-9891.

29. Prat, I.; Company, A.; Corona, T.; Parella, T.; Ribas, X.; Costas, M. Assessing the impact of electronic and steric tuning of the ligand in the spin state and catalytic oxidation ability of the Fe(II)(Pytacn) family of complexes. *Inorg. Chem.* **2013**, *52*, 9229-9244.

30. England, J.; Gondhia, R.; Bigorra-Lopez, L.; Petersen, A. R.; White, A. J.; Britovsek, G. J. Towards robust alkane oxidation catalysts: electronic variations in non-heme iron(ii) complexes and their effect in catalytic alkane oxidation. *Dalton. Trans.* **2009**, 5319-5334.

31. Thorarinsdottir, A. E.; Gaudette, A. I.; Harris, T. D. Spin-crossover and high-spin iron(ii) complexes as chemical shift $^{(19)}$F magnetic resonance thermometers. *Chem. Sci.* **2017**, *8*, 2448-2456.

32. Boukheddaden, K.; Ritti, M. H.; Bouchez, G.; Sy, M.; Dîrtu, M. M.; Parlier, M.; Linares, J.; Garcia, Y. Quantitative Contact Pressure Sensor Based on Spin Crossover Mechanism for Civil Security Applications. *J. Phys. Chem. C* **2018**, *122*, 7597-7604.

33. Gütlich, P.; Gaspar, A. B.; Garcia, Y. Spin state switching in iron coordination compounds. *Beilstein. J. Org. Chem.* **2013**, *9*, 342-391.

34. Robert, F.; Naik, A. D.; Tinant, B.; Robiette, R.; Garcia, Y. Insights into the origin of solid-state photochromism and thermochromism of N-salicylidene anils: the intriguing case of aminopyridines. *Chem.* **2009**, *15*, 4327-4342.

35. Danielsson, P. E. Euclidean distance mapping. *Computer Graphics and Image Processing* **1980**, *14*, 227-248.

36. Ward, J. H. Jr Hierarchical Grouping to Optimize an Objective Function. *J. Am. Stat. Assoc.* **1963**, *58*, 236-244.

37. Lim, S. H.; Feng, L.; Kemling, J. W.; Musto, C. J.; Suslick, K. S. An optoelectronic nose for the detection of toxic gases. *Nat. Chem.* **2009**, *1*, 562-567.

38. Scott, S. M.; James, D.; Ali, Z. Data analysis for electronic nose systems. *Microchim. Acta.* **2006**, *156*, 183-207.

39. Plaisance, H.; Blondel, A.; Desauziers, V.; Mocho, P. Hierarchical cluster analysis of carbonyl compounds emission profiles from building and furniture materials. *Build. Environ.* **2014**, *75*, 40-45.

Table of contents